

This is the peer reviewed version of the following article:

Performances and robustness of a fluorescent sensor for nearly-neutral pH measurements in healthcare / Cattini, Stefano; Truzzi, Stefano; Accorsi, Luca; Rovati, Luigi. - In: IEEE TRANSACTIONS ON INSTRUMENTATION AND MEASUREMENT. - ISSN 0018-9456. - 69:10(2020), pp. 7658-7665. [10.1109/TIM.2020.2984964]

Terms of use:

The terms and conditions for the reuse of this version of the manuscript are specified in the publishing policy. For all terms of use and more information see the publisher's website.

10/01/2026 02:55

Performances and robustness of a fluorescent sensor for nearly-neutral pH measurements in healthcare

Stefano Cattini, *Member, IEEE*, Stefano Truzzi, Luca Accorsi and, Luigi Rovati, *Member, IEEE*,

Abstract—The capability to measure pH is fundamental in many fields ranging from healthcare and agri-food, to chemistry and industrial applications. In medicine, the possibility of in-line and real-time monitoring critical care analytes such as pH is recognized to provide relevant information for the diagnosis and treatment of a variety of disorders and would be of considerable support for the management of extracorporeal (blood) circulation (ECC). In this paper, we theoretically and experimentally investigate the performances and the robustness of a fluorescent sensor we recently proposed for the in-line and real-time monitoring of blood pH in extracorporeal circulation (ECC). Thanks to the low-cost and biocompatibility, the proposed sensor can be used for the in-line and real-time monitoring of the pH of fluids especially in applications such as healthcare where safe and low-cost disposable are required for all parts in contact with the patient. The reported results demonstrate that the proposed sensor allows achieving significant robustness to unevennesses in the production process of the sensing element.

Index Terms—Ratiometric fluorescent sensor, pH measurement, Biomedical measurement, Healthcare, Extracorporeal circulation (ECC), Hemodialysis, Hemofiltration, Extracorporeal membrane oxygenation (ECMO).

I. INTRODUCTION

In spite of the long history of pH measurement, many problems are still open and new measuring systems are continuously developed to meet measurement needs. Indeed, pH monitoring is fundamental in many fields ranging from medicine and agri-food, to chemistry and industrial applications [1]–[5].

In healthcare, the acid-base status of critically ill patients is often altered, thus blood pH is one of the most important parameters to be monitored in the emergency room, recovery room and intensive care unit. In particular, the possibility of real-time and in-line monitoring blood pH would be of significant support for the management of extracorporeal blood circulation (ECC). ECC includes a set of different medical procedures in which the patient's blood flows outside the body for therapies such as blood purification or heart and lungs temporary replacement as in cardiac surgery.

Given the interest in blood pH monitoring, many measurement methods and measuring systems have been presented in the literature in the last years i.e. [1], [6]–[14]. However, as discussed in more detail in our recent paper [5], nowadays no

measurement method has been able to provide safe, economical, accurate and reliable estimates of pH in the bloodstream to be used routinely during ECC treatments, thus blood pH is generally not monitored during ECC treatments. To overcome all the above limitations, in our recent paper [5], we proposed and described a measuring system composed of a disposable fluorescent sensor and a non-disposable optical-head for the in-line and real-time monitoring of blood-pH in extracorporeal-circulation (ECC). In such a paper [5], we described the proposed measuring instrument and measurement method, we report about a preliminary investigation on biocompatibility and, finally, we reported the results obtained by simulating with bovine blood an about 6 h ECC treatment. In this paper, we investigate and describe the performances and the robustness of the proposed sensor to unevennesses in the production process.

As will be demonstrated, such performances and robustness are mainly due to both the measurement method and model and, the developed sensing element. As a result, in the following, section II describes the sensing element, derives the measurement model and, reports the experimental activities carried out for the sensor characterization. The obtained results are reported in section III and conclusions are drawn in section IV.

II. MATERIALS AND METHODS

The following subsections, briefly describe the sensing element (subsection II-A), analyze in detail the measurement model (subsection II-B), and, give a detailed account of the experimental activities carried out to characterize the proposed sensing element (subsection II-C).

A. The sensing element

The proposed sensing element is based on HPTS (8-Hydroxypyrene-1,3,6-trisulfonic acid trisodium salt) an inexpensive and nontoxic ratiometric pH indicator. The fluorophore is fixed to the polymeric substrate by using anion exchange microbeads and a biocompatible polyurethane hydrogel according to the 6-step production process described in our recent paper [5]. An “out of scale” cross-section of the sensing element is shown in Fig. 1.

Excluding the polymeric substrate, the cost of the raw materials used for a single sensor is about a tenth of a euro.

B. Measurement model

According to the optical properties of HPTS that will be shown in subsection III-B and the following demonstration,

S. Cattini and L. Rovati are with the Department of Engineering “Enzo Ferrari”, University of Modena and Reggio Emilia, Via Vivarelli 10, 41125, Modena, Italy. All the authors are with the Science & Technology Park for Medicine, TPM, Democenter Foundation Mirandola, Modena, Italy e-mail: stefano.cattini@unimore.it

Manuscript received XXX, XXX; revised XXXX.

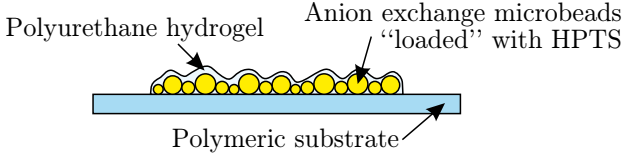


Fig. 1. Out of scale cross-section of the proposed sensor. The yellow circles represent the anion exchange microbeads “loaded” with HPTS. The microbeads are fixed to the polymeric substrate by the polyurethane hydrogel. The sensing element is thus composed of the microbeads “loaded” with HPTS and the polyurethane hydrogel.

the pH value can be estimated from the ratio of the fluorescent optical powers emitted by the sensor in small wavelength band around $\lambda_{em} \approx 520$ nm while exciting the sensor at wavelengths $\lambda_{ex-1} \approx 405$ nm and $\lambda_{ex-2} \approx 475$ nm, respectively.

The fluorescent radiance generated by the sensor is proportional to the excitation power that is absorbed by the fluorophore [15], [16]. Since the sensing element is substantially composed of a monolayer of anion exchange microbeads loaded with HPTS (see Fig. 3), according to Fig. 2 and assuming the sensing element to be illuminated by a monochromatic infinite plane wave with irradiance $I_0(x, y)$ impinging orthogonally to the surface of the sensor, the overall irradiance absorbed by a small portion of the sensing element having thickness $d(x, y)$ and infinitesimal area $d\sigma$ can be estimated according to the Beer-Lambert’s law as:

$$I_0(x, y) - I_T(x, y) = I_0(x, y) \cdot [1 - 10^{-A(x, y)}], \quad (1)$$

where I_T is the irradiance of the beam after crossing the sensor and, A is the (overall) absorbance [17]:

$$\begin{aligned} A(\lambda, x, y) &\stackrel{def}{=} \log_{10} \left[\frac{I_0(\lambda, x, y)}{I_T(\lambda, x, y)} \right] = \frac{1}{2.303} \cdot \ln \left[\frac{I_0(\lambda, x, y)}{I_T(\lambda, x, y)} \right] \\ &= \left\{ \sum_{i=1}^N \epsilon_i(\lambda) \cdot [C_i] \right\} \cdot d \cdot DPF + G + A_{sub}(\lambda) \\ &= A_{sens}(\lambda, x, y) + A_{sub}(\lambda, x, y), \end{aligned} \quad (2)$$

where λ is the wavelength, $N = 3$ is the number of chromophores — light-absorbing species — composing the sensing element (HPTS, anion exchange microbeads and, polyurethane hydrogel), $[C_i](x, y)$ and $\epsilon_i(\lambda)$ are the concentration and the molar absorption coefficient of the i^{th} -chromophore composing the sensor, $DPF(\lambda, x, y)$ is the differential pathlength factor that takes into account potentially extended pathlength due to scattering, $G(\lambda, x, y)$ represents potential losses due to scattering and, $A_{sub}(\lambda, x, y)$ and $A_{sens}(\lambda, x, y)$ represent the absorbances of the polymeric substrate and the sensing element, respectively. In (2) the chromophores concentrations $[C_i](x, y)$ have been supposed to be uniform throughout the thickness $d(x, y)$.

It is important to notice that the fluorescent intensity is not due to the overall absorbance of the sensing element A_{sens} , but it is proportional to the excitation power that is absorbed by the fluorophore only:

$$A_{HP}(\lambda, x, y) = \epsilon_{HP}(\lambda) \cdot [C_{HP}](x, y) \cdot d(x, y) \cdot DPF(x, y), \quad (3)$$

where ϵ_{HP} and $[C_{HP}]$ are the molar absorption coefficient and the molarity of HPTS, respectively.

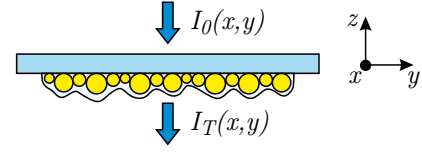


Fig. 2. The fluorescent intensity generated by the sensor is proportional to the excitation power that is absorbed by the fluorophore. I_0 and I_T are the irradiances impinging on the polymeric substrate and after crossing the sensor.

Hence, the overall optical power P_F relative to the fluorescence generated by the sensor in a small bandwidth around the λ_{em} wavelength once it is illuminated (excited) by a beam having a small bandwidth around the wavelength λ_{ex} and irradiance I_0 is:

$$P_F = \Phi_E \cdot k \cdot \iint_{x, y} I_0(x, y) \cdot [1 - e^{-2.303 \cdot A_{HP}(x, y)}] dx dy, \quad (4)$$

where $\Phi_E(\lambda_{ex}, \lambda_{em}, pH)$ is the fluorescence quantum yield — the ratio of photons emitted at λ_{em} through fluorescence to photons absorbed at λ_{ex} , — $k(\lambda_{ex}, \lambda_{em})$ is a constant that takes into account the different energies of photons at λ_{ex} and λ_{em} . Expanding in series the exponential in (4) and keeping only the zero and first-order terms, (4) becomes:

$$P_F \approx \Phi_E \cdot k \cdot \iint_{x, y} I_0(x, y) \cdot 2.303 \cdot A_{HP}(x, y) dx dy. \quad (5)$$

Note that the approximation of (5) is valid for $A_{HP} < 1$. Indeed, as will be shown in Fig. 3, the proposed sensing element is very thin, thus the absorption is little as it will be shown in subsection III-A (note that, according to (3) and (8) the absorbance of the fluorophore A_{HP} is only a fraction of the overall absorbances showed in Fig. 5).

Supposing uniform illumination — $I_0(x, y) = I_0$ — from (3) and (5) the overall fluorescence power P_F is:

$$P_F \approx \Phi_E \cdot k \cdot 2.303 \cdot \epsilon_{HP} \cdot I_0 \cdot \iint_{x, y} [C_{HP}] \cdot d \cdot DPF dx dy. \quad (6)$$

As a result, the ratio between the overall optical powers P_{F-2} and P_{F-1} emitted at the emission wavelength λ_{em} once the sensor is respectively excited at the wavelengths λ_{ex-2} and λ_{ex-1} is substantially insensitive to changes in sensor thickness and fluorophore concentration:

$$\begin{aligned} \frac{P_{F-2}}{P_{F-1}} &= \frac{\Phi_{E-2} \cdot k_2 \cdot \epsilon_{HP}(\lambda_{ex-2}) \cdot I_0(\lambda_{ex-2})}{\Phi_{E-1} \cdot k_1 \cdot \epsilon_{HP}(\lambda_{ex-1}) \cdot I_0(\lambda_{ex-1})} \\ &= \frac{\Phi_{E-2} \cdot k_2 \cdot \epsilon_{HP}(\lambda_{ex-2}) \cdot P_{sen}(\lambda_{ex-2})}{\Phi_{E-1} \cdot k_1 \cdot \epsilon_{HP}(\lambda_{ex-1}) \cdot P_{sen}(\lambda_{ex-1})}, \end{aligned} \quad (7)$$

where $\Phi_{E-2} = \Phi_E(\lambda_{ex-2}, \lambda_{em})$, $\Phi_{E-1} = \Phi_E(\lambda_{ex-1}, \lambda_{em})$, $k_2 = k(\lambda_{ex-2}, \lambda_{em})$, $k_1 = k(\lambda_{ex-1}, \lambda_{em})$ and, P_{sen} is the overall excitation optical power equal to the product between the I_0 irradiance and the sensor area in the (x, y) plane. Equation (7) has been obtained assuming that the scattering coefficient varies little between λ_{ex-1} and λ_{ex-2} . Indeed, the DPF is due by both the concentration and the scattering coefficient of the scatterers. Since the scatterers are the same both for λ_{ex-1} and λ_{ex-2} and, the two wavelengths are not very far apart, we

approximated $DPF(\lambda_{ex-1}, x, y) \approx DPF(\lambda_{ex-2}, x, y)$.

For pH-sensitive ratiometric fluorophores such as HPTS, Φ_{E-1} , Φ_{E-2} , $\epsilon_{HP}(\lambda_{ex-1})$ and $\epsilon_{HP}(\lambda_{ex-2})$ are known to vary as a function of the pH. Therefore, from (7) it is evident that the ratio between the fluorescent powers emitted by the sensing elements depends on both the pH and, the irradiances $I_0(\lambda_{ex-1})$ and $I_0(\lambda_{ex-2})$. As a result, it is important to monitor and compensate potential drift of the excitation powers.

C. Sensor characterization

Sensor characterization has been aimed at investigating the performances and robustness of the proposed sensor and measurement method to unevennesses in the production of the sensors. The properties of the fluorescent sensing element have been investigated by analyzing and comparing the performances of $N_s = 6$ sensors produced following the procedure previously described in subsection II-A and using a 6-wells multi-well plate (model 657160 by Greiner) as substrate. A picture of the sensors is shown in Fig. 3.

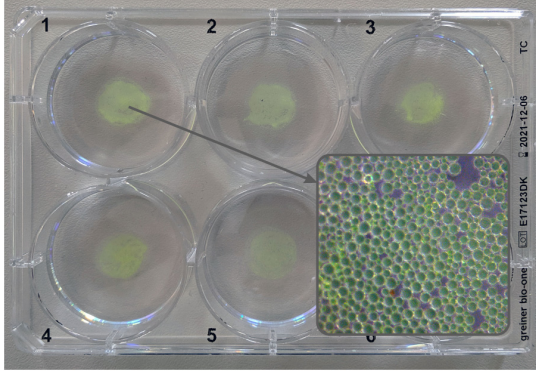


Fig. 3. Picture of the $N_s = 6$ sensors produced following the procedure described in subsection II-A and using a 6-wells multi-well plate (model 657160 by Greiner) as substrate. The zoom shows the anion exchange microbeads “loaded” with HPTS and fixed to the substrate by the polyurethane hydrogel (microbeads sizes declared by the manufacturer: [200, 400] mesh).

Sensors have been investigated by analyzing the absorbance and fluorescence spectra as a function of the pH of the medium — the measurand. To modify the pH, wells were filled with 5 ml phosphate-buffered saline (PBS) solutions at different pH. The pH of the PBS solutions was estimated by using a pH electrode (model HI9125, Hanna). PBS has been preferred to blood since blood-pH is known to vary with the blood-pCO₂. Hence, blood-pH would have varied over time due to exposure to air, giving rise to a relevant uncertainty on the pH value of the sample.

Then, spectral absorbance and fluorescence were analyzed by using a Multimode Plate Reader (MPR, model EnSpire 2300 by PerkinElmer). In particular, as shown in Fig. 4, the absorbance has been investigated by measuring the attenuation of the light beam traversing the layered structure realized by the substrate, the sensor and, the PBS. On the other hand, the fluorescence has been investigated by exciting and measuring from the bottom of the well.

To guarantee repeatability conditions, for each pH value the absorbance and fluorescence spectra were measured thermostating the sensors at 27 °C using the MPR and, waiting a

warm-up time of 5 minutes after the sensors were inserted into the MPR — during the warm-up, sensors were gently shaken by the MPR. Indeed, both the pH of PBS and the fluorescence quantum yield Φ_E are known to vary as a function of the temperature and, preliminary tests revealed that in our test conditions (thickness of the sensors and temperatures of the ambient, the PBS and, the measuring chamber of the MPR) 5 minutes were sufficient to guarantee that the sensing element reached the steady-state condition both in terms of temperature and H^+ ions concentration. Then, both the absorbance and the fluorescent spectra were recorded by setting the MPR to an intensity equal to 10 flashes.

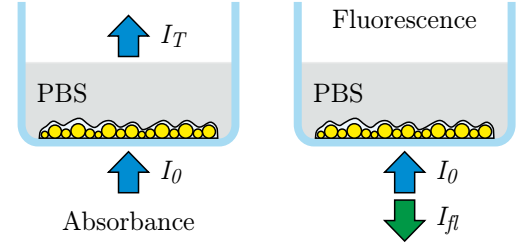


Fig. 4. The absorbance has been investigated by measuring the attenuation of the light beam traversing the three-layer structure realized by the substrate, the sensor and the PBS. I_0 and I_T are irradiances impinging and transmitted after traversing the three layers. On the other hand, fluorescence has been investigated by exciting the sensor and measuring the fluorescence from the bottom of the well. I_{fl} is the fluorescence irradiance. d_s and d_{PBS} are the (mean) thicknesses of the sensor and the PBS layer, respectively.

1) Substrate absorbances and inter-sensors uniformity:

Absorbance spectra have been investigated by using the MPR previously described and modifying the pH of the PBS solution filling each well.

It is important to notice that absorbance spectra allow to both investigate the optical properties of the fluorescent sensor and, to investigate the inter-sensors uniformity. Indeed, according to (2), the overall absorbance A of a monochromatic and collimated light beam of irradiance I_0 traversing the three-layer structure realized by the substrate, the sensor and the PBS can be estimated according to the Beer-Lambert's law as:

$$A = A_{sub} + A_{sens} + A_{PBS}, \quad (8)$$

where, A_{sub} , A_{sens} and A_{PBS} are the absorbances of the substrate, the sensor and the PBS. According to subsection II-A, the sensing element is composed of 3 chromophores, namely the HPTS, the hydrogel and, anion exchange microbeads. Since the molar absorption coefficient of HPTS ϵ_{HP} is known to vary as a function of the pH, while the others quantities basically do not, it is possible to define the following quantity:

$$\begin{aligned} \gamma(\lambda, pH_1, pH_2) &= A(\lambda, pH_2) - A(\lambda, pH_1) \\ &\approx [C_{HP}] \cdot d_s \cdot DPF \cdot \Delta\epsilon_{HP}(\lambda, pH_1, pH_2), \end{aligned} \quad (9)$$

where $[C_{HP}]$ is the (mean) concentration of the fluorophore (HPTS), d_s is the (mean) thickness of the sensing element, DPF is the (mean) differential pathlength factor that takes into account potential scattering, and

$$\Delta\epsilon_{HP}(\lambda, pH_1, pH_2) = \epsilon_{HP}(\lambda, pH_2) - \epsilon_{HP}(\lambda, pH_1). \quad (10)$$

In (9) the variation in PBS thickness has been neglected as the thickness of the sensing element is negligible compared to that of PBS.

Since $\Delta\epsilon_{HP}$ is a property of HPTS, thus the same for all the 6 sensors, differences between the γ values obtained from the absorbances of the 6 sensors reveal differences in the HPTS concentrations $[C_{HP}]$, thicknesses d_s and/or scattering (DPF) between the sensors. Thus, inter-sensors uniformity has been investigated analyzing

$$\Delta\gamma(\lambda, pH_1, pH_2) = \frac{\gamma(\lambda, pH_1, pH_2) - \gamma_{mean}(\lambda, pH_1, pH_2)}{\gamma_{mean}(\lambda, pH_1, pH_2)}, \quad (11)$$

and

$$s_\gamma = \sqrt{\frac{1}{N_s - 1} \sum_{i=1}^{N_s} [\gamma(i) - \gamma_{mean}]^2} \cdot (|\gamma_{mean}|)^{-1}, \quad (12)$$

where $s_\gamma(\lambda, pH_1, pH_2)$ is the relative experimental standard deviation, $\gamma(i)$ is the γ value respective to the i^{th} -sensor and, $\gamma_{mean}(\lambda, pH_1, pH_2)$ is the mean γ recorded from the $N_s = 6$ sensors. Equation (11) has been divided by γ_{mean} so that to remove the contribution of $\Delta\epsilon_{HP}$, thus providing an estimate of how much the current sensor differs in percentage from the “average sensor” in terms of fluorophore concentration, thickness and, scatterers.

2) *Substrate fluorescence and calibration curve*: As previously shown in Fig. 4, for each sensor the fluorescence has been investigated by using the MPR, and exciting and measuring the sensor from the bottom of the well. It is important to notice that the spectra provided by spectrofluorimeters are automatically rescaled by the excitation power used by the spectrofluorimeter to obtain the fluorescence signal. Thus, the fluorescence spectra provided by the Multimode Plate Reader at λ_{ex-1} and λ_{ex-2} are corrected with respect to variation of P_{sen} in (7). Then, unevennesses in the fluorescence signals generated by the various sensors have been investigated similarly to what was done for the analysis of the absorbance spectra. Hence, for each of the $N_s = 6$ sensors we estimated:

$$\Delta P(i, \lambda_{em}, \lambda_{ex}, pH) = \frac{P(i) - P_{mean}}{P_{mean}}, \quad (13)$$

and,

$$s_P = \sqrt{\frac{1}{N_s - 1} \sum_{i=1}^{N_s} [P(i) - P_{mean}]^2} \cdot (P_{mean})^{-1}, \quad (14)$$

where λ_{em} and λ_{ex} are the emission and excitation wavelengths, $P(i, \lambda_{em}, \lambda_{ex}, pH)$ is the fluorescence optical power recorded from the i^{th} -sensor and, $P_{mean}(\lambda_{em}, \lambda_{ex}, pH)$ and $s_P(\lambda_{em}, \lambda_{ex}, pH)$ are the mean and the relative experimental standard deviation of the P recorded from the $N_s = 6$ sensors.

Moreover, according to subsection II-B, from the analysis of the fluorescence spectrum, it is possible to estimate the pH of the solution. Thus, in accordance with (7), for each of the 6 sensors we estimate the ratios R :

$$R(i, pH) = \frac{P(i, \lambda_{em}, \lambda_{ex-2}, pH)}{P(i, \lambda_{em}, \lambda_{ex-1}, pH)}, \quad (15)$$

and the sigmoid obtained as a function of the pH. Then, the calibration function $pH_{est}(R)$ has been estimated by reversing such sigmoid function as described in subsection III-B.

3) *Sensitivity and pK_a* : The pK_a of the fluorophore defines the sensitivity and the measuring interval of the sensor [18]. Thus, it is important to know and match the pK_a of the indicator to the pH of the measurand [18]. pK_a of HPTS is known in the literature e.g. $pK_a \approx 7.30$ in 0.066 M phosphate buffers at 22 °C [18]. However, pK_a depends on several quantities such as the ionic strength, and the dielectric constant of the surrounding medium [19]. Hence, it is important to determine the pK_a of HPTS once incorporated in the polyurethane hydrogel and anion exchange microbeads.

The pK_a of the sensor in PBS has been estimated as the pH value for which the second-order derivative of the R values as a function of the pH of the medium is equal to zero — the inflection point [19]:

$$pK_a = pH : \frac{\partial^2 R}{\partial^2 pH} = 0. \quad (16)$$

Then, the sensitivity η of the sensor has been investigated as the derivative of the R values as a function of the pH of the medium:

$$\eta = \frac{\partial R}{\partial pH}. \quad (17)$$

III. RESULTS

A. Substrate absorbances and inter-sensors uniformity

As an example, Fig. 5 shows the absorbance spectra obtained from one of the $N_s = 6$ sensors realized using the multi-well plate as described in subsection II-A.

According to subsection II-C, inter-sensors uniformity has been investigated analyzing the γ parameter defined in (9). Fig. 6 shows the $\Delta\gamma$ values obtained from the $N_s = 6$ sensors considering $pH_1 = 4.11$ pH and $pH_2 = 9.50$ pH. As shown in Fig. 6, the $\Delta\gamma$ obtained by the “handmade” sensors revealed significant differences. Thus, according to (11), sensors have significant differences in terms of HPTS concentrations $[C_{HP}]$, thicknesses d_s and/or scattering (DPF). Indeed, according to (12) we obtained $s_\gamma \approx 40\%$ for $\lambda = 408$ nm and $s_\gamma \approx 38\%$ for $\lambda = 464$ nm (the two peak wavelengths in the absorption spectra). Nevertheless, thanks to the use of a ratiometric fluorophore, the sensors have almost the same ratio R as it will be shown in subsection III-B.

B. Substrate fluorescence and calibration curve

As an example, Fig. 7 shows the fluorescence spectra obtained from one of the $N_s = 6$ sensors realized using the multi-well plate as described in subsection II-A.

Fig. 8 and 9 show the ΔP and s_P values obtained by analyzing the $N_s = 6$ sensors according to (13) and (14). According to the results obtained by analyzing the absorbance spectra and previously shown in Fig. 6, also the results relative to fluorescence spectra shown in Fig. 8 and 9 reveal significant inter-sensors differences.

Despite the significant inter-sensors differences shown in Fig. 6, 8 and, 9, the ratiometric analysis described in (15)

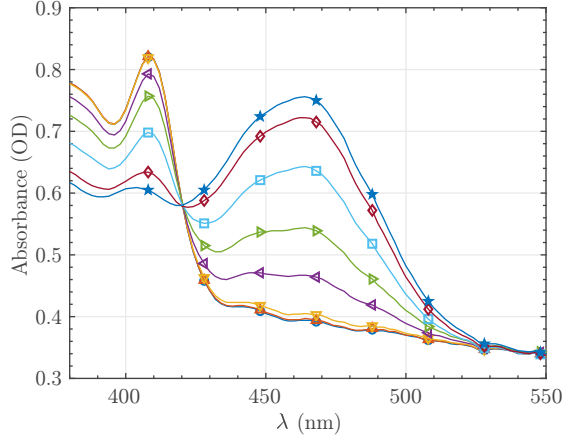


Fig. 5. Absorbance spectra as a function of the pH of the PBS solution obtained from one of the $N_s = 6$ sensors realized using the multi-well plate (PBS solution 1X, at 27 °C). $pH = 4.11$ (\circ), $pH = 5.11$ (\triangle), $pH = 6.13$ (∇), $pH = 7.10$ (\diamond), $pH = 7.50$ (\triangleright), $pH = 8.00$ (\square), $pH = 8.58$ (\diamond), and, $pH = 9.50$ (\star). As expected, spectra at low pH values — (\circ) and (\triangle) — substantially overlap.

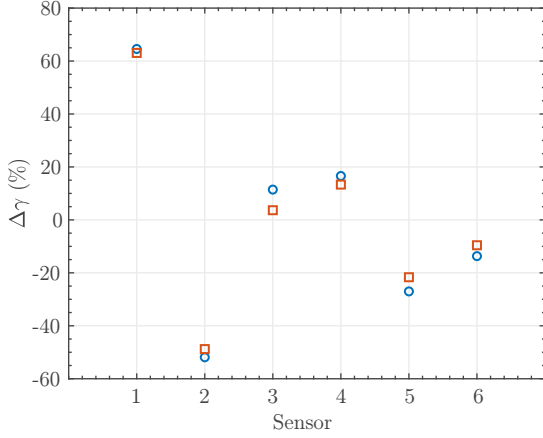


Fig. 6. $\Delta\gamma$ values obtained from the $N_s = 6$ sensors considering $pH_1 = 4.11$ pH and $pH_2 = 9.50$ pH (PBS solution 1X, at 27 °C). The reported values have been obtained according to (11) and analyzing the two peaks in Fig. 5. In particular, (\circ) have been obtained by analyzing $\lambda = 408$ nm and (\square) have been obtained by analyzing $\lambda = 464$ nm.

allows to greatly limit the negative effects due to such inter-sensors differences. Fig. 10 shows the mean R values and the respective experimental standard deviations of the mean $s_{R-mean} = s_R/\sqrt{N_s}$ obtained from the sensors changing the pH of the PBS solutions filling the wells:

$$R_{mean}(pH) = \frac{1}{N_s} \sum_{i=1}^{N_s} R(i, pH) , \quad (18)$$

$$s_R(pH) = \sqrt{\frac{1}{N_s - 1} \sum_{i=1}^{N_s} [R(i) - R_{mean}]^2} ,$$

where $R(i, pH)$ is the R value obtained from the i^{th} -sensor. In particular, according to (15), each $R(i, pH)$ has been obtained exciting the sensing element at $\lambda_{ex-1} = 405$ nm and $\lambda_{ex-2} = 475$ nm and, recording the fluorescence power P emitted in the band $\lambda_{em} = [515, 525]$ nm. Fig. 12 shows the relative experimental standard deviations (s_R/R_{mean}) of the

R values obtained from the $N_s = 6$ sensors.

As previously described in subsection II-C, the ratio R allows estimating the pH of the solution. The function obtained by reversing the sigmoid shown in Fig. 10 is:

$$pH = \alpha_3 - \log_{10} \left(\frac{\alpha_2 - \alpha_1}{R - \alpha_1} - 1 \right) \cdot \alpha_4^{-1} , \quad (19)$$

where $\alpha_1 = 6.5 \cdot 10^{-3}$, $\alpha_2 = 1.867$, $\alpha_3 = 6.920$ and, $\alpha_4 = 0.635$. Note that (19) has real solutions only for $\alpha_1 < R < \alpha_2$. Therefore, given the limited sensitivity that would be obtained for pH values at the ends of the sigmoid and the interest in nearly-neutral pH , we have defined the calibration function as follows:

$$\begin{aligned} pH_{est} &= f(R) \\ &= \alpha_3 - \log_{10} \left(\frac{\alpha_2 - \alpha_1}{R - \alpha_1} - 1 \right) \cdot \alpha_4^{-1} \Leftarrow R_{min} < R < R_{max} \\ &= 10 \Leftarrow R \geq R_{max} \\ &= 4 \Leftarrow R \leq R_{min} . \end{aligned} \quad (20)$$

where $R_{min} = 32.17 \cdot 10^3$ and $R_{max} = 1.8469$. By applying (20) to the experimental R values it is possible to estimate both the relative errors

$$\epsilon(i, pH) = \frac{pH - pH_{est}(i, pH)}{pH_{est-mean}(pH)} , \quad (21)$$

and, the relative experimental standard deviations s_{pH-est} of the pH_{est} values:

$$s_{pH-est}^2(pH) = \frac{\sum_{i=1}^{N_s} [pH_{est}(i, pH) - pH_{est-mean}(pH)]^2}{(N_s - 1) \cdot [pH_{est-mean}(pH)]^2} \quad (22)$$

where $pH_{est}(i, pH)$ is the estimate obtained from the i^{th} -sensor at pH and $pH_{est-mean}(pH)$ is the mean. The obtained results are shown in Fig. 11 and 12.

Note that, since Fig. 6 gives an idea of how much the 6 sensors differ from the “average sensor” in terms of fluorophore concentration, thickness and, scatterers (see subsection II-C), while Fig. 11 and 12 show the percentage errors and the relative experimental standard deviations obtained by using the same calibration function for all the 6 sensors, by comparing Fig. 6, 11 and, 12, it is possible to obtain a visual estimate of the “robustness” of the ratiometric method to unevenness in the production process.

C. Sensitivity and pK_a

Fig. 13 and 14 show the η and $\partial^2 R / \partial^2 pH$ values obtained from the sigmoid function shown in Fig. 10. As expected, the pK_a obtained in Fig. 14 is equal to the α_3 obtained in (19). As shown in Fig. 10, 13 and 14, the measuring interval is about $[4, 10]$ pH and the maximum sensitivity is achieved for nearly-neutral pH values where $\eta \approx 0.7$ pH⁻¹. Thus, the maximum sensitivity in PBS at 27 °C is achieved for a pH value slightly different from the physiological pH value of the blood — $\approx [7.35, 7.45]$ pH.

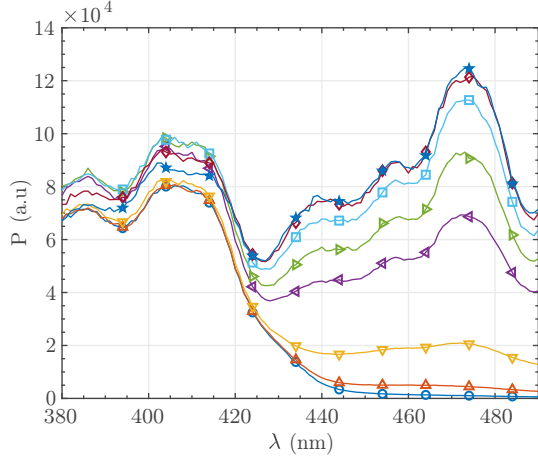


Fig. 7. Fluorescence spectra obtained exciting the sensor at various λ and measuring the relative fluorescence power P emitted at $\lambda_{em} = 520$ nm. Measurements have been performed varying the pH of the solution filling the well (PBS solution 1X, at 27 °C). $pH = 4.11$ (\circ), $pH = 5.11$ (\triangle), $pH = 6.13$ (∇), $pH = 7.10$ (\triangleleft), $pH = 7.50$ (\triangleright), $pH = 8.00$ (\square), $pH = 8.58$ (\diamond) and, $pH = 9.50$ (\star).

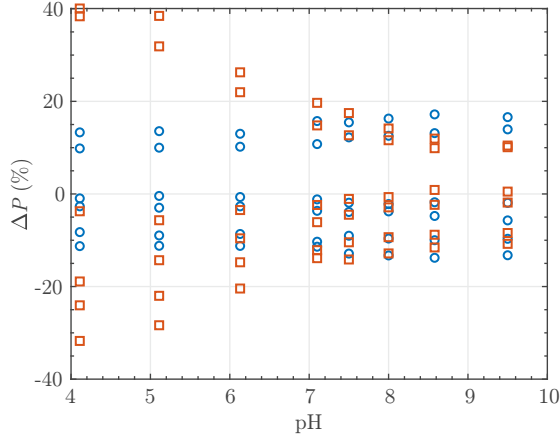


Fig. 8. ΔP values obtained from the $N_s = 6$ sensors (PBS solution 1X, at 27 °C). The reported values have been obtained according to (13) and analyzing the two peaks in Fig. 7. In particular, (\circ) and (\square) have been obtained by analyzing the fluorescence of the $N_s = 6$ sensors at $\lambda \approx 405$ nm and $\lambda \approx 475$ nm, respectively.

IV. DISCUSSIONS AND CONCLUSIONS

The acid-base status of critically ill patients is often altered, hence blood pH is one of the most important parameters to be monitored. As an example, as previously introduced, the possibility of in-line and real-time monitoring blood pH would be of considerable support for the management of ECC. However, nowadays no measurement method has been able to provide safe, economical, accurate and reliable estimates of pH in the bloodstream to be used routinely during ECC treatments [5], thus blood pH is generally not monitored during such treatments.

To overcome such a limitation, in our recent paper [5] we propose a measuring system composed of a disposable fluorescent sensing element and a non-disposable optical-head aimed at the contactless reading of the sensor. Indeed, optical techniques offer an extremely interesting measurement

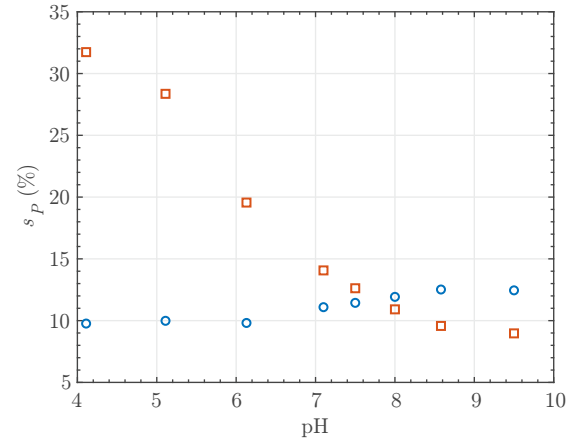


Fig. 9. s_P values obtained from the $N_s = 6$ sensors as a function of the pH (PBS solution 1X, at 27 °C). The reported values have been obtained according to (14) and analyzing the two peaks in Fig. 7. In particular, (\circ) and (\square) have been obtained by analyzing the fluorescence of the $N_s = 6$ sensors at $\lambda \approx 405$ nm and $\lambda \approx 475$ nm, respectively.

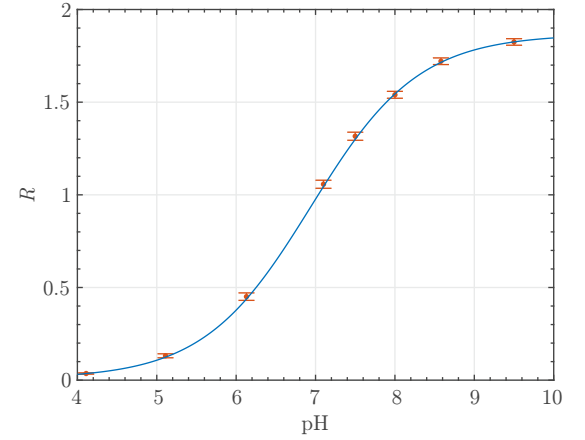


Fig. 10. Ratios R at various pH values (PBS solution 1X, 27 °C). Dots (\bullet) and error bars represent the R_{mean} and the experimental standard deviations of the mean obtained from the $N_s = 6$ sensors. The line ($—$) represents the sigmoid function obtained from the fitting of the R_{mean} values.

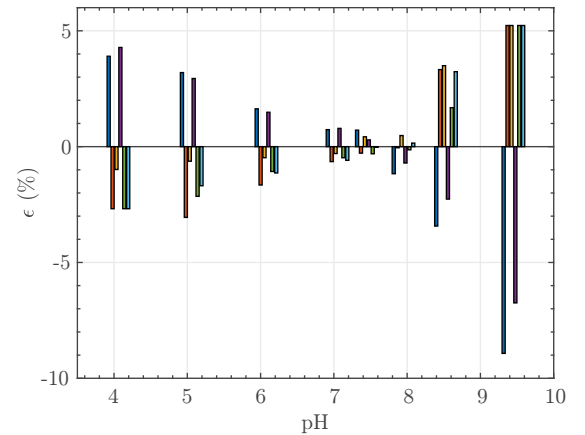


Fig. 11. Relative errors ϵ obtained from the $N_s = 6$ sensors as a function of the pH of the solution. For each pH value N_s bars are shown.

principle for the in-line and real-time monitoring of blood

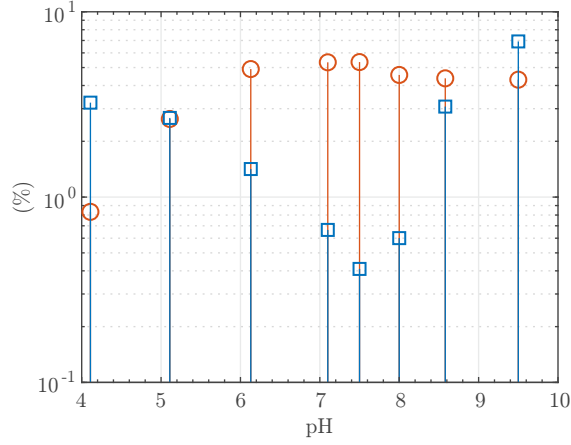


Fig. 12. Relative experimental standard deviations s_R/R_{mean} (○) and, s_{pH-est} (□) obtained from the $N_s = 6$ sensors as a function of the pH of the solution.

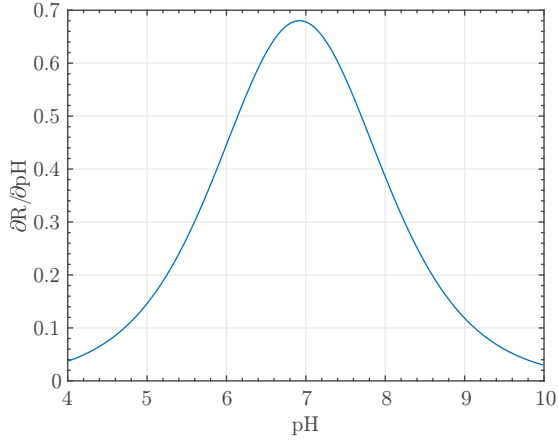


Fig. 13. Sensitivity η obtained from the sigmoid function shown in Fig. 10 according to (17).

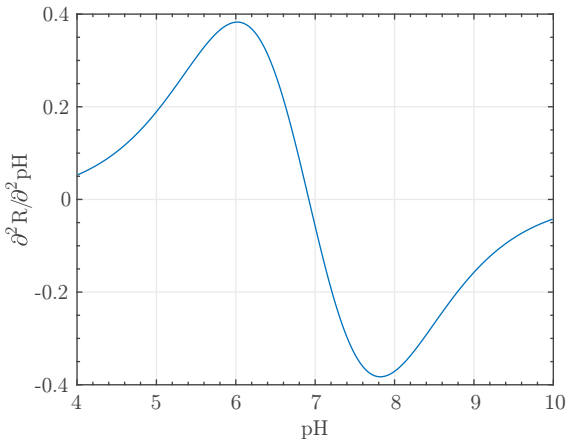


Fig. 14. $\partial^2 R / \partial^2 pH$ values obtained from the sigmoid function shown in Fig. 10. According to (16), $pK_a = 6.92$ pH.

parameters in ECC. As a matter of fact, in our previous articles, we have benefited from optics in ECC for the in-line measurement of blood flow [20], monitoring of the urea clearance [21] and, measurement of the hemolysis [22], [23].

In this paper, we theoretically and experimentally investigate the performances of the sensing element introduced in our recent paper [5]. According to the results reported in such a paper [5], the sensing element is both safe for the patient — preliminary tests performed according to ISO 10993-1:2018 revealed no biological hazards — and, capable of in-line and real-time measure the blood-pH in ECC — a 6 hours ECC treatment simulated using bovine blood revealed a maximum deviation with respect to the reference measuring instrument of about 0.01 pH while blood-pH was repeatedly varied in the range [6.95, 7.45] pH. In this paper, we mainly focus our attention on the analysis of the robustness of the sensor to unevenness in the production process. According to the reported results, the proposed measurement method and sensor are robust with respect to non-uniformity of the production process. Indeed, despite the sensors revealed composition differences of up to 60% (Fig. 6 and 8), the R parameter showed variations of a few percentage points (Fig. 12). Such R variations give rise to very limited variations in the estimates of the pH values. In fact, as shown in Fig. 12, the obtained relative experimental standard deviations of the pH_{est} values were generally of the order of a few percentage points and, below 1% in the nearly-neutral region.

Note that, according to (5), to fully exploit the robustness of ratiometric fluorophores to variations of the concentration of the fluorophores $[C_{HP}](x, y)$ and thickness $d(x, y)$ of the sensing element, the irradiance $I_0(x, y)$ of the exciting beams must be uniform — $I_0(x, y) = I_0$. Similarly, uniform concentration of the fluorophores and thickness results in a sensors robustness to uneven irradiance $I_0(x, y)$.

Concluding, the proposed sensing element offers the possibility to transform polymeric tubes and containers into sensors that can be read contactless from outside, offering robust in-line and real-time monitoring of the pH of the inside fluid. Thanks also to the low-cost and biocompatibility [5], the proposed sensor can be used for the monitoring of the pH of fluids especially in applications such as healthcare where safe and low-cost disposable are required for all parts in contact with the patient. Hence, it may allow supporting the many healthcare applications from the emergency room to the recovery room and the intensive care where it is important to monitor the altered acid-base status of critically ill patients.

REFERENCES

- [1] O. Korostynska, K. Arshak, E. Gill, and A. Arshak, "Review paper: Materials and techniques for in vivo pH monitoring," *IEEE Sensors Journal*, vol. 8, no. 1, pp. 20–28, Jan 2008.
- [2] S. Bhadra, W. Blunt, C. Dynowski, M. McDonald, D. J. Thomson, M. S. Freund, N. Cicek, and G. E. Bridges, "Fluid embeddable coupled coil sensor for wireless ph monitoring in a bioreactor," *IEEE Transactions on Instrumentation and Measurement*, vol. 63, no. 5, pp. 1337–1346, May 2014.
- [3] S. Yuan, H. Wang, S. H. Hesari, S. Shamsir, and S. K. Islam, "A monolithic low-power highly linear ph measurement system with power conditioning system for medical application," *IEEE Transactions on Instrumentation and Measurement*, pp. 1–9, 2018.
- [4] Y. Liao and H. Lai, "Investigation of a wireless real-time ph monitoring system based on ruthenium dioxide membrane ph sensor," *IEEE Transactions on Instrumentation and Measurement*, pp. 1–9, 2019.

- [5] S. Cattini, L. Accorsi, S. Truzzi, and L. Rovati, "On the development of an instrument for in-line and real-time monitoring of blood-pH in extracorporeal-circulation," *IEEE Transactions on Instrumentation and Measurement*, vol. -, no. -, pp. -, - 2019. [Online]. Available: <http://dx.doi.org/10.1109/TIM.2019.2961499>
- [6] D. D. Zhou, "Chapter 10 - microelectrodes for in-vivo determination of pH," in *Electrochemical Sensors, Biosensors and their Biomedical Applications*, X. Zhang, H. Ju, and J. Wang, Eds. San Diego: Academic Press, 2008, pp. 261 – 305.
- [7] W. Jin, L. Wu, Y. Song, J. Jiang, X. Zhu, D. Yang, and C. Bai, "Continuous intra-arterial blood pH monitoring by a fiber-optic fluorosensor," *IEEE Transactions on Biomedical Engineering*, vol. 58, no. 5, pp. 1232–1238, May 2011.
- [8] L. Ferrari, L. Rovati, P. Fabbri, and F. Pilati, "Continuous haematic pH monitoring in extracorporeal circulation using a disposable fluorescence sensing element," *Journal of Biomedical Optics*, vol. 18, no. 2, pp. 1 – 10, 2013. [Online]. Available: <https://doi.org/10.1117/1.JBO.18.2.027002>
- [9] Z. Q. Tou, C. C. Chan, and S. Leong, "A fiber-optic pH sensor based on polyelectrolyte multilayers embedded with gold nanoparticles," *Measurement Science and Technology*, vol. 25, no. 7, p. 075102, may 2014.
- [10] B. Schyrr, S. Pasche, E. Scolan, R. Ischer, D. Ferrario, J.-A. Porchet, and G. Voirin, "Development of a polymer optical fiber pH sensor for on-body monitoring application," *Sensors and Actuators B: Chemical*, vol. 194, pp. 238 – 248, 2014.
- [11] N. Deepa and A. B. Ganesh, "Sol-gel based portable optical sensor for simultaneous and minimal invasive measurement of pH and dissolved oxygen," *Measurement*, vol. 59, pp. 337 – 343, 2015. [Online]. Available: <http://www.sciencedirect.com/science/article/pii/S0263224114004527>
- [12] M. C. Frost and M. E. Meyerhoff, "Real-time monitoring of critical care analytes in the bloodstream with chemical sensors: Progress and challenges," *Annual Review of Analytical Chemistry*, vol. 8, no. 1, pp. 171–192, 2015. [Online]. Available: <https://doi.org/10.1146/annurev-anchem-071114-040443>
- [13] D. Wencel, A. Kaworek, T. Abel, V. Efremov, A. Bradford, D. Carthy, G. Coady, R. C. N. McMorro, and C. McDonagh, "Optical sensor for real-time pH monitoring in human tissue," *Small*, vol. 14, no. 51, p. 1803627, 2018. [Online]. Available: <https://onlinelibrary.wiley.com/doi/abs/10.1002/sml.201803627>
- [14] S. Jamasb, "Continuous monitoring of pH and blood gases using ion-sensitive and gas-sensitive field effect transistors operating in the amperometric mode in presence of drift," *Biosensors*, vol. 9, no. 1, 2019. [Online]. Available: <http://www.mdpi.com/2079-6374/9/1/44>
- [15] G. Henderson, "The effects of absorption and self-absorption quenching on fluorescent intensities," *Journal of Chemical Education*, vol. 54, no. 1, pp. 57–59, 1977.
- [16] P. John, W. McCarthy, and J. Winefordner, "Applications of signal-to-noise theory in molecular luminescence spectrometry," *Analytical Chemistry*, vol. 38, no. 13, pp. 1828–1835, 1966.
- [17] L. Ferrari, L. Rovati, M. P. Costi, R. Luciani, A. Venturelli, and S. Cattini, "Feasibility study on a measurement method and a portable measuring system to estimate the concentration of cloxacillin and β -lactamase in milk," *Journal of Sensors*, vol. 2017, p. 5742359, 2017. [Online]. Available: <https://doi.org/10.1155/2017/5742359>
- [18] I. Johnson and M. Spence, Eds., *pH Indicators*, 11th ed. Life Technologies, 2010, ch. 20.
- [19] J. Reijenga, A. van Hoof, A. van Loon, and B. Teunissen, "Development of methods for the determination of pKa values," *Analytical Chemistry Insights*, vol. 8, no. 1, pp. 53–71, 2013. [Online]. Available: <https://doi.org/10.4137%2FACI.S12304>
- [20] S. Cattini, M. Norgia, A. Pesatori, and L. Rovati, "Blood flow measurement in extracorporeal circulation using self-mixing laser diode," in *Optical Diagnostics and Sensing X: Toward Point-of-Care Diagnostics*, G. L. Coté, Ed., vol. 7572, International Society for Optics and Photonics. SPIE, 2010, pp. 62 – 72. [Online]. Available: <https://doi.org/10.1117/12.840240>
- [21] L. Rovati and S. Cattini, "UV-LEDs for monitoring dialysis adequacy," *IEEE Transactions on Instrumentation and Measurement*, vol. 58, no. 5, pp. 1720–1726, May 2009. [Online]. Available: <https://doi.org/10.1109/TIM.2008.2009410>
- [22] S. Cattini, L. Rovati, M. Bernabei, D. Cianciavichchia, P. Monari, and A. Sicuri, "A simple measuring system for early detection of haemolysis during haemodialysis," in *Instrumentation and Measurement Technology Conference (I2MTC) Proceedings, 2014 IEEE International*, May 2014, pp. 282–287. [Online]. Available: <https://doi.org/10.1109/I2MTC.2014.6860753>
- [23] S. Cattini and L. Rovati, "An optical technique for real-time monitoring of hemolysis during hemodialysis," *IEEE Transactions on Instrumentation and Measurement*, vol. 65, no. 5, pp. 1060–1069, 2016. [Online]. Available: <https://doi.org/10.1109/TIM.2015.2490939>